

A LONG, HARD LOOK AT THE LOW-HARD STATE IN ACCRETING BLACK HOLES

J. M. MILLER¹, J. HOMAN², D. STEEGHS³, M. RUPEN⁴, R. W. HUNSTEAD⁵, R. WIJNANDS⁶, P. A. CHARLES^{7,8}, A. C. FABIAN⁹

Subject headings: Black hole physics – relativity – stars: binaries (GX 339–4) – physical data and processes: accretion disks

Draft version May 10, 2018

ABSTRACT

We present the first results of coordinated multi-wavelength observations of the Galactic black hole GX 339–4 in a canonical low–hard state, obtained during its 2004 outburst. *XMM-Newton* observed the source for 2 revolutions, or approximately 280 ksec; *RXTE* monitored the source throughout this long stare. The resulting data offer the best view yet obtained of the inner accretion flow geometry in the low–hard state, which is thought to be analogous to the geometry in low-luminosity active galactic nuclei. The *XMM-Newton* spectra clearly reveal the presence of a cool accretion disk component, and a relativistic Fe K emission line. The results of fits made to both components strongly suggest that a standard thin disk remains at or near to the innermost stable circular orbit, at least in bright phases of the low–hard state. These findings indicate that potential links between the inner disk radius and the onset of a steady compact jet, and the paradigm of a radially–recessed disk in the low–hard state, do not hold universally. The results of our observations can best be explained if a standard thin accretion disk fuels a corona which is closely related to, or consistent with, the base of a compact jet. In a brief examination of archival data, we show that Cygnus X-1 supports this picture of the low/hard state. We discuss our results within the context of disk–jet connections and prevailing models for accretion onto black holes.

1. INTRODUCTION

The nature of accretion onto black holes at low fractions of the Eddington mass accretion rate has been the topic of considerable observational and theoretical attention. Especially in the *Chandra* and *XMM-Newton* era, improved sensitivity has permitted the study of very faint sources. *Chandra* observations of Sgr A* have begun to probe the nature of the accretion flow onto this super-massive black hole at $L_X/L_{Edd} \simeq 10^{-10}$ (Baganoff et al. 2003). Yet, the nature of accretion onto black holes even at $L_X/L_{Edd} \simeq 10^{-2}$ remains uncertain. Galactic black hole transients are especially good laboratories in which to study the manner in which flows change with mass accretion rate. In particular, clear changes in the mass accretion rate and flow geometry are thought to be marked by changes in X-ray colors, flux, fast X-ray variability, and multi-wavelength properties as a source transitions from a high–soft state to the low–hard state (for reviews, see McClintock & Remillard 2005, Homan & Belloni 2004).

Building upon analysis of spectral states by Miyamoto et al. (1995), Homan et al. (2001) showed that simple variations in the implied mass accretion rate alone cannot account for the state transitions and properties observed in the 1998–1999 outburst of XTE J1550–564. It was noted that at least one additional parameter appears to have a profound influence on the flux and properties of an accreting black hole. Homan et al. (2001) suggested that the second parameter might be related to

the size of the corona. The size of the corona might naturally be regulated by the radius of the inner edge of an optically-thick accretion disk. Alternatively, the inner disk radius may not change, or may be less important than independent characteristics of the corona.

A common, paradigmatic model of how accretion flows change with state and mass accretion rate was given by Esin et al. (1997). In that model, high–soft states are dominated by a standard thin accretion disk, but in the low–hard state the inner disk is radially truncated and replaced by an advection-dominated accretion flow. The same essential geometry is thought to describe quiescent phases. The fundamental assumption of a radially recessed accretion disk may find some support in the low disk reflection fractions which are sometimes measured in the low/hard state (e.g., Gierlinski et al. 1997). Beloborodov (1999) proposed a very different picture for the nature of state transitions and the accretion flow geometry in the low–hard state. In this model, black hole states are driven by the height of magnetic flares above a disk which remains at the innermost stable circular orbit (ISCO). These flares would serve to feed a mildly relativistically–outflowing corona. Low disk reflection fractions do not signal a recessed disk in this model, but result from mild beaming of the hard X-ray flux away from the disk. Merloni & Fabian (2002) have discussed a similar picture of the low/hard state, based on magnetically–dominated coronae.

¹Department of Astronomy, University of Michigan, 500 Church Street, Ann Arbor, MI 48109, jonmm@umich.edu

²Kavli Institute for Astrophysics and Space Research, MIT, 77 Massachusetts Avenue, Cambridge, MA 02139

³Harvard-Smithsonian Center for Astrophysics, 60 Garden Street, Cambridge, MA 02138

⁴Array Operations Center, National Radio Astronomy Observatory, 1003 Lopezville Road, Socorro, NM 87801

⁵School of Physics A29, University of Sydney, NSW 2006, Australia

⁶Astronomical Institute “Anton Pannekoek”, Kruislaan 403, University of Amsterdam, 1098 SJ Amsterdam, NL

⁷School of Physics & Astronomy, University of Southampton, Highfield Campus, Southampton SO17 1BJ, UK

⁸South African Astronomical Observatory, PO Box 9, Observatory 7935, Cape Town, South Africa

⁹Institute of Astronomy, University of Cambridge, Madingley Road, Cambridge CB3 0HA, UK

In order to better understand the nature of the low–hard state, we proposed to make a deep observation of GX 339–4 in the low–hard state with *XMM-Newton*. GX 339–4 is a well-known recurrent transient, which harbors a low-mass donor star and a black hole with a mass of at least $5.8 M_{\odot}$ (Hynes et al. 2003). The distance to GX 339–4 is likely 8 kpc (Zdziarski et al. 2004; also see Hynes et al. 2004). It has been well-studied at all wavelengths, but notable recent results include the detection of transient jets with $v/c > 0.9$ (Gallo et al. 2004), evidence for a high black hole spin parameter based on a prominent Fe $K\alpha$ emission line in its X-ray spectrum (Miller et al. 2004a, 2004b), and evidence for broad-band jet emission based on multi-wavelength observations (Homan et al. 2005). In the sections that follow, we present the results of X-ray spectral fits to GX 339–4 in its low–hard state.

2. OBSERVATIONS AND DATA REDUCTION

XMM-Newton observed GX 339–4 during revolutions 782 and 783, for a total exposure of approximately 280 ksec. Extensive simultaneous radio observations were obtained with the Australia Telescope Compact Array (ATCA). Optical and IR monitoring observations were obtained simultaneously at the South African Astronomical Observatory (SAAO) using the 1.0m and IRSF 1.4m telescopes. In addition, the Optical Monitor (OM) onboard *XMM-Newton* provided simultaneous V band observations at high time resolution. The full results of this multi-wavelength observing program will be presented in a separate paper, and are only mentioned briefly in this work.

The “medium” EPIC optical blocking filter was used during the observations made with *XMM-Newton*, as the optical magnitude of the source was expected to be fainter than $V = 6$. The prime instrument for this observation was the EPIC-pn camera, which was run in timing mode. Unfortunately, the source flux was too high for this mode, and the camera experienced photon pile-up. We note that *XMM-Newton* has since revised the flux and count rate limits for timing mode to be a factor of two lower. The RGS units were operated in the standard “spectroscopy” mode, and the OM was operated in “fast” mode. Our analysis of the data from these instruments will be presented in separate work.

The EPIC-MOS1 and EPIC-MOS2 cameras were operated in the standard “full frame” mode. The MOS cameras have a nominal operational range of 0.2–10.0 keV. Data from these cameras was reduced using SAS version 6.5. The EPIC-MOS camera good time started on 2004–03–16 at 16:23:41 (TT). Although these cameras also suffered photon pile-up, it was possible to extract robust spectra and lightcurves from these cameras by using annular extraction regions to avoid the piled-up core of the bright source image (spatial information is not preserved in EPIC-pn “timing” mode). The spectra obtained from these cameras are the centerpiece of the analysis detailed in this work. Using the SAS tool “xmmselect” we filtered the MOS1 and MOS2 event lists to include event grades 1–12 and “flag=0”. The event lists were screened against times with high instrumental flaring. This resulted in net MOS1 and MOS2 exposure times of 81 ksec (each) during revolution 782, and 59 ksec (each) during revolution 783. Using the xmmselect tool “epatplot”, we compared the spectra extracted in a number of annuli to the expected distribution of energy and event grades with radius. Via this procedure, it was found that extracting source counts in annuli between 18–120” resulted in spectra free from pile-up. Background spectra were taken from a 60”

circle near the corner of the central chip on each MOS camera. The “backscale” tool was used to correctly normalize the source and background events. Finally, the FTOOL “grppha” was used to require at least 10 counts per bin in each spectrum. Redistribution matrix files (rmfs) and ancillary response files (arfs) for each spectrum were calculated using the tools “rmfgen” and “arfgen”.

During the long *XMM-Newton* stare, simultaneous X-ray snapshots were obtained with *RXTE*, in order to better-define the broad-band X-ray continuum emission and to characterize the timing properties of the source. These observations were reduced using the packages and tools available in HEASOFT version 6.0. As this paper is focused on the results of fits made to the *XMM-Newton*/EPIC-MOS spectra, we have chosen to focus on one representative *RXTE* observation. Observation 90118-01-06-00 began on 2004-03-17 at 12:03:12 (TT). After standard screening (e.g., against SAA intervals), net PCA and HEXTE exposures of 2.2 ksec and 0.8 ksec were obtained.

PCU-2 is the best-calibrated PCU in the *RXTE*/PCA. A spectrum from PCU-2 was extracted from data taken in “Standard2” mode, providing full coverage of the 2.0–60.0 keV bandpass in 129 channels every 16 seconds. Data from all the Xe gas layers in PCU-2 were combined. Background spectra were made using the FTOOL “pcabackest” using the latest “bright source” background model. An instrument response file was obtained using the tool “pcarsp”. It is well-known that fits to PCA spectra of the Crab with a simple power-law model reveal residuals as large as 1%, but adding 1% errors to PCA data is often an over-estimate (see, e.g., Rossi et al. 2005). Using the tool “grppha”, we added 0.6% systematic errors to the PCU-2 spectra. The HEXTE-A cluster was operated in the standard “archive” mode, which has a time resolution of 32 s and covers the 10.0–250.0 keV band with 61 channels. We extracted a background-subtracted spectrum from the HEXTE-A cluster, and an associated instrument response file, using the standard procedures.

The *XMM-Newton*/EPIC-MOS cameras nominally cover the 0.2–10.0 keV band. A preliminary inspection of the data revealed small but significant deviations at the lowest and highest energy bounds. These likely result from small anomalies in the instrument response function for the annuli we have used; we therefore restricted our spectral analysis to the 0.7–9.0 keV band. The low energy bins in the *RXTE*/PCA are not calibrated as well as the central part of the bandpass, and the same is true for the higher energy portion of the bandpass. Therefore, we restricted our analysis of the PCU-2 spectrum to the 2.8–25.0 keV band. Prior experience with PCA spectra suggests that the strongest Xe L edge is not fully accounted for by the detector response; in all fits to the PCU-2 spectrum detailed below, an edge at 4.78 keV with $\tau = 0.1$ was included to account for this small effect. We restricted our analysis of the HEXTE-A spectrum to energies above 20 keV. The HEXTE-A spectrum has little signal above 100 keV, so this energy was set as an upper bound on all fits. XSPEC version 11.3.2 was used to analyze the *XMM-Newton* and *RXTE* spectra. All errors reported in this work are 90% confidence errors obtained by allowing all parameters to vary, unless otherwise noted.

3. ANALYSIS AND RESULTS

3.1. ATCA Radio Observations

Throughout the long stare obtained with *XMM-Newton*, GX 339–4 was observed with the Australia Telescope Compact Array (ATCA) at 4.8 and 6.2 GHz, for the bulk of 14–

hour observing runs between 16 and 19 March 2004. The data were reduced in the standard fashion using the Miriad (e.g., Sault & Killeen 2004) and AIPS (e.g., Greisen 2005) software packages. The resulting images showed GX 339–4 to be a point source with no obvious extension, at a resolution of $6.1 \times 5.2''$ (4.8 GHz), and $5.7 \times 4.9''$ (6.2 GHz). The mean flux densities (referenced to the standard flux calibrator PKS B1934–638) were 5.3 ± 0.05 mJy (4.8 GHz) and 5.7 ± 0.05 mJy (6.2 GHz), where the error bars reflect the rms noise in the images from individual days, and there is no sign of strong variability.

In summary, ratio of radio flux to X-ray flux, the radio spectral index ($\alpha = +0.3 \pm 0.1$, $S_\nu \propto \nu^\alpha$), and the lack of strong variability (on the order of 0.1 mJy from day to day), are all typical of radio emission in the low–hard state. Such radio emission is generally interpreted as the signature of a steady, compact jet (e.g., Fender 2005).

3.2. *RXTE* Timing Analysis

An inspection of the *RXTE* X-ray light curves revealed strong flaring, superimposed on a relatively stable base flux level. The flares occurred on a time scale of a few tens of seconds and the flare maxima occasionally reached count rates close to eight times that of the base level. Power spectra were created from the GoodXenon data (total energy band, 2–60 keV), with frequency ranges of 128^{-1} –1024 Hz. The power spectra were normalized according to Belloni and Hasinger (1990) and Miyamoto et al. (1991), and the Poisson level was subtracted following the method described in Klein-Wolt et al. (2004).

Two broad peaks could be identified in the power spectrum of each of the *RXTE* observations (a representative power spectrum is shown in Figure 1). One Lorentzian peaks around 0.05 Hz, corresponding to the strong flaring that is directly visible in the light curves, and a second, broader feature peaks around 2 Hz. The low-frequency peak power could be fit well with one Lorentzian, with a Q-value (i.e. frequency divided by full-width-at-half-maximum) of ~ 0.3 and a fractional rms amplitude of $\sim 30\%$. This feature can be identified with the break that is seen in the hard state power spectra of, e.g. Cyg X-1 (Belloni & Hasinger 1990). Two Lorentzians were needed to fit the feature at higher frequencies, peaking around 0.5 Hz (Q fixed to 0, $\text{rms} \approx 20\%$) and 2.5 Hz (Q ≈ 0.15 , $\text{rms} \approx 25\%$). The total strength of the variability in the 128^{-1} –64 Hz range is about 47–51%. The variability properties in our observations are consistent with those of the canonical hard state.

3.3. Preliminary *RXTE* Spectral Analysis

We made a preliminary study of the *RXTE* PCU-2 and HEXTE-A spectra. The spectra were fit jointly within XSPEC, utilizing a constant to account for normalization differences. The continuum is well fit by a very simple model consisting of a power-law modified by absorption (using the “phabs” model with N_H fixed at 4.0×10^{21} atoms cm^{-2} , Miller et al. 2004a). Only a broad Fe $K\alpha$ emission line (see Figure 2) prevents the simple power-law model from being a formally acceptable fit ($\chi^2/\nu = 385.7/76$). Using this continuum model, we measure a photon index of $\Gamma = 1.50(2)$, and a normalization of $0.21(1)$ ph cm^{-2} s^{-1} keV^{-1} at 1 keV. This corresponds to an unabsorbed flux of 5.33×10^{-9} erg cm^{-2} s^{-1} in the 3–100 keV band, or a luminosity of 4.1×10^{37} erg s^{-1} (or $L_X \leq 0.05 L_{\text{Edd}}$) for a distance of 8 kpc. While there is some evidence for subtle curvature in the high energy spectrum that is consistent with

disk reflection, it is too weak to be significant. Power-law models with an exponential high-energy cut-off and broken power-law models do not provide significant improvements to the continuum fit.

A simple power-law fit in the 20–100 keV band gives an energy flux of 2.5×10^{-9} erg cm^{-2} s^{-1} , and a photon flux of 3.6×10^{-2} ph cm^{-2} s^{-1} . This places our simultaneous X-ray and radio flux measurements in the middle of the radio–X-ray flux correlation Corbel et al. (2000) found to hold in the low–hard state of GX 339–4, and further indicates that we observed GX 339–4 in a standard low–hard state.

3.4. Preliminary *XMM-Newton* Spectral Analysis

We next explored simple continuum fits to the *XMM-Newton*/EPIC-MOS spectra. We fit the four spectra (MOS1 and MOS2 from revolutions 782 and 783) jointly, allowing a normalizing constant to float between the spectra. A simple power-law model like that which adequately described the *RXTE* spectra was unable to fit the continuum in the *XMM-Newton* spectra, due to a strong soft flux excess.

The presence of a strong soft excess in the *XMM-Newton* spectra does not represent a flaw in the performance or calibration of the instruments aboard either observatory. Rather, the soft flux excess is merely not required in the *RXTE* band, due to its effective low-energy bound of 3 keV. When a low energy threshold of 3.0 keV is chosen to match that of *RXTE*, a simple power-law model adequately describes the continuum in the *XMM-Newton* spectra. Extending this fit down to 0.7 keV reveals that the soft excess is very significant below 2–3 keV in the *XMM-Newton* spectra. This effect is illustrated in Figure 3.

For any reasonable continuum model (a continuum consisting of one or two additive components, which can be strongly constrained by the data), fits reveal strong evidence for a relativistic iron line arising from the inner disk (see Figures 4, 5, and 6).

Studies of black hole X-ray binary outbursts with *RXTE* have documented falling accretion disk flux and apparent temperature through the outburst decay (e.g., Park et al. 2004; see also McClintock & Remillard 2005). Below a certain disk temperature and flux level, however, *RXTE* is simply unable to detect disk emission. In plotting additive component fluxes measured across an outburst with *RXTE*, then, it is not uncommon to see a sudden disappearance of the disk flux. However, it is unlikely that disk emission simply turns off at this point. It is also unlikely that *RXTE* can provide robust constraints on the nature of the disk in low-temperature, low-flux phases. It is most likely that the soft excess we have discovered with *XMM-Newton* is due to emission from an optically-thin, geometrically-thick accretion disk, and that *XMM-Newton* is much better-suited to such measurements.

3.5. Joint Spectral Fits with Simple Models

We explored a number of fits with different disk components and hard components, to demonstrate that the disk and disk line components truly arise from an accretion disk, and are not modeling artifacts. We note that no fits to the *XMM-Newton*/EPIC-MOS spectra, by themselves or in combination with *RXTE* spectra, are formally acceptable. This is due to the presence of residual instrumental response deficiencies near 1 keV and 2 keV. Similar response issues have been documented previously (e.g., Miller et al. 2004b), and do not complicate efforts to obtain strong constraints on the nature of the

accretion flow. The results of this analysis are particularly robust because the fits span the 0.7–100.0 keV range, providing excellent constraints on the continuum emission, and because of the extraordinary depth of our observations.

For each model fit to the spectra, a normalizing constant was included to allow for flux differences between *XMM-Newton* and *RXTE*. This constant was fixed at unity for each of the MOS cameras, but component normalizations (not, e.g., temperature or photon index) were allowed to float between the cameras to account for more minor flux variations (2–5% or less). As the PCA and HEXTE spectra are not suited to constraining the column density or the parameters of any cool disk components, all soft component parameters were tied to the values obtained for the MOS-1 spectrum from revolution 782. This procedure is reasonable as global disk parameters should only vary on the viscous timescale (see, however, Belloni et al. 1997 and Vadawale et al. 2003), which is longer than the timescale of our observations. Apart from their normalizations, all emission line and hard component parameters in fits to the PCA and HEXTE spectra were linked with parameters measured via the MOS spectra. The same normalizations were used for both the PCA and HEXTE spectra, again by tying these parameters together.

The parameters measured with four plausible continuum models are listed in Table 1 (see also Figures 4, 5, and 6). The most important results obtained from these fits are that a cool $kT \simeq 0.3$ keV disk (cool compared to the $kT \simeq 1$ –2 keV disks observed in high flux states; see McClintock & Remillard 2005) and a strong relativistic iron line are required in each model. Using the F-test, we find that both components are individually required at much more than the 8σ level of confidence. Adding a smeared edge component (“smedge” in XSPEC; although unphysical, it is sometimes included to approximate a disk reflection continuum) did not significantly improve the fits. This may indicate that the disk reflection is very weak (see below).

In the three continuum models wherein the disk radius may be inferred from the additive disk component, each fit points to an inner disk extending close to or within $6 GM/c^2$. We made fits with two different disk models to ensure that any such finding is not strongly dependent on the model chosen. Inner disk radii inferred via disk continuum fits are notoriously unreliable, as they depend on the hard component assumed, the inner disk boundary condition, the column density, spectral hardening, and other effects (see Zimmerman et al. 2004 for a discussion of different disk models; see Merloni, Fabian, & Ross 2000 for a detailed discussion of hardening effects). In all four models, however, the “Laor” relativistic line model points to a disk which may extend to $3 GM/c^2$. This finding may provide additional evidence that GX 339–4 harbors a spinning black hole (Miller et al. 2004a, 2004b).

Three of the models considered include additive model components; the fourth model (the “bulk motion Comptonization” or BMC model; Shrader & Titarchuk 1999) is a single continuum which attempts to account for up-scattering from a disk self-consistently. The fact that a relativistic disk line component is still strongly required in fits with the bulk motion Comptonization (BMC) model, and that the line parameters are consistent with those measured via the additive models, signals that the line itself is not an artifact of using additive components to fit the X-ray continuum. Moreover, the measured values of the line are similar in each model. We note that the disk temperature derived via the BMC model ($kT = 0.26(1)$ keV) is at most

0.1 keV lower than values obtained via the fits with additive components, and that the best fit is obtained with the canonical “diskbb” plus “power-law” continuum. This finding may indicate that the disk emission is not strongly Comptonized, and that any coronal geometry may not strongly distort our view of the inner disk.

Simple theoretical considerations strongly support interpreting the cool soft excess we have observed as an accretion disk. For standard thin accretion disks, $T \propto \dot{M}^{1/4}$ (assuming that $L \propto \dot{M}$; e.g., Frank, King, & Raine 2002). Based on an *XMM-Newton* observation of GX 339–4 in the “very high” or “steep power-law state”, Miller et al. (2004b) report an apparent disk temperature of $kT = 0.76$ keV for an unabsorbed disk flux of 1.4×10^{-8} erg cm² s⁻¹ (0.5–10.0 keV). In the low–hard state observation described in this work, the unabsorbed disk flux is 10% of the total, or 2.7×10^{-10} erg cm² s, and the range of disk temperatures is $kT = 0.27$ –0.38 keV. The ratio of apparent temperatures and mass accretion rates is fully consistent with the $T \propto \dot{M}^{1/4}$ relation expected for standard thin accretion disks which extend to the innermost stable circular orbit.

While the results of these fits with simple models clearly demonstrate the presence and robustness of a broad Fe K emission line, it is also worth noting that this line profile clearly reveals the importance of dynamical broadening. The line profile (see Fig. 5 and Fig. 6) is similar to the classic, two-horn profile originally found in the spectrum of MCG–6–30–15 with *ASCA* (Tanaka et al. 1995). In one sense, this shape more clearly reveals that the line is broadened by dynamical processes, than extremely skewed lines: at least in the case of Seyfert AGN, the extreme red wing in some lines may be partially affected by (though not due to) low-energy absorption (e.g., Vaughan & Fabian 2004). Similarly, this line shape, and the absence of Fe XXV and Fe XXVI absorption lines in the spectrum, serve to rule-out high energy absorption as a contribution to the line shape and flux (e.g., Done & Gierlinski 2006). Prior work has discussed alternative broadening mechanisms extensively. It has been shown that Comptonization is extremely unlikely to cause the broadening observed (e.g., Fabian et al. 1995, Reynolds & Wilms 2000). Velocity shifts and/or scattering effects in a jet or outflow (e.g., Titarchuk, Kazanas, & Becker 2003) have also been shown to be extremely unlikely sources of line broadening (Fabian et al. 1995; Miller et al. 2004a).

The fits we have made with relativistic line models imply a low inner disk inclination in GX 339–4. An inclination of $i \simeq 18^\circ$ is consistent with the fits obtained, and prior fits to the line profile (Miller et al. 2004a,b). If the binary is viewed at this low inclination, an implausibly high black hole mass would be implied (Hynes et al. 2003). However, the inner disk and binary plane can be misaligned in black hole binaries. In at least two systems (GRO J1655–40 and V4641 Sgr), the inner disk inclination implied by relativistic jets and the orbital plane of the binary are known to be significantly different (see, e.g., Maccarone 2002). It is likely that GX 339–4 is another such system. A velocity of $0.9c$ is sufficient to create the Doppler boosting needed to make the approaching jet visible and the receding jet invisible within an angle of 26° , in radio observations of jets launched from GX 339–4 (Gallo et al. 2004). This implies that the inner disk is viewed at an inclination of 26° or less, since the jet velocity may be higher and the beaming angle tighter (Gallo et al. 2004). The inclination implied by our spectral fits is broadly consistent with that inferred from jets. If the inclination is instead fixed at a value as high as 55° , the inner radius

implied by fits with Laor line components is still within $6 r_g$, although this inclination forces a significantly worse fit statistically.

3.6. Joint Spectral Fits with Disk Reflection Models

As the results of spectral fits with simple models clearly reveal an accretion disk and relativistic disk line, we next attempted fits with disk reflection models. The methodology outlined above was employed, with regard to multiplicative constants and normalizations. Reflection models predict that an Fe K emission line is merely the most prominent part of the interaction between hard X-rays and the accretion disk; more subtle effects include a small flux decrement above the line energy, and a “reflection hump” which normally peaks between 20–30 keV. Fitting disk reflection models, then, represents the most self-consistent means of treating the relativistic line and hard X-ray continuum.

We considered two disk reflection models: the “constant density ionized disk” model with solar abundances (CDID; Ballantyne, Iwasawa, & Fabian 2001), and “pexriv” (Magdziarz & Zdziarski 1995). It is expected that the CDID model is more physical, in that it is suited to high disk ionization and includes the effects of Comptonization on absorption edges. We therefore used the results of fits with the CDID model as a guide when fitting “pexriv”, which has more free parameters. In particular, we fixed the disk temperature and ionization parameter within “pexriv” to values consistent with those obtained when fitting the CDID model. It should also be noted that whereas the CDID model explicitly includes Fe line emission, pexriv does not, and an additional Laor line component was included in fits with pexriv. Finally, reflection models are calculated in the fluid frame, and to match the observed spectrum, a reflection model must be convolved with the relativistic effects expected in the inner disk around a black hole. These effects expected around a spinning black hole are described by the “laor” line model, and so we convolved the CDID and pexriv models with the laor line element in all spectral fits. This procedure is referred to as relativistic blurring. In the case of fits with pexriv, the blurring parameters were simply tied to the independent line component parameters.

Fitting blurred reflection models is computationally intensive; the fits themselves and error scans can take several days to calculate even on high-end workstations. We therefore took the pragmatic step of only including the *XMM-Newton*/EPIC-MOS spectra from revolution 782. The spectra from revolution 782 have more counts than those from 783, as there was more observing time free from instrumental flaring.

It is useful to compare our current results to those obtained from reflection fits to bright hard states. The CDID and pexriv reflection models were fit to the *XMM-Newton*/EPIC-pn spectra of XTE J1650–500 and GX 339–4 in the “very high” or “steep power-law” state. In those cases, reflection fractions ($f \propto \Omega/2\pi$) broadly consistent with unity and high disk ionizations ($\log(\xi) \simeq 4.0$, and higher) were measured (Miller et al. 2002a; Miller et al. 2004b). These prior results imply that in each case, an ionized thin accretion disk extended to the innermost stable circular orbit (ISCO).

The complete set of parameters obtained with the blurred constant density ionized disk and pexriv models are detailed in Table 2, and shown in Fig. 7 and Fig. 8. Fits to the low-hard state spectra from GX 339–4 suggest a moderate disk ionization, $\log(\xi) \simeq 3.0$ ($\xi = L_X/nr^2$, where n is the hydrogen number density). This is consistent with the low apparent disk temper-

ature we have measured, and with the hard ionizing flux levels that are observed in the low-hard state. The low reflection fractions we have measured ($f \simeq 0.2-0.3$) are consistent with prior results obtained in the low-hard state (e.g., Gierlinski et al. 1997).

Whereas low disk reflection fractions could previously be explained in terms of a radially-recessed accretion disk, our data appear to rule out such an explanation. The apparently inconsistent findings of a disk remaining at the innermost stable circular orbit, and a low reflection fraction, can be reconciled if the hard X-ray emission is mildly beamed away from the accretion disk. As with the case of phenomenological models discussed above and detailed in Table 1, we found that the parameter values obtained with reflection models are not strongly dependent on the assumed inner disk inclination.

From the source luminosity and the ionization parameter measured via the CDID model, it is possible to estimate the density of the reflecting medium. Assuming an inner radius of $3.0 r_g$, a density of $n \sim 10^{21} \text{ cm}^{-3}$ is implied. Further assuming a radiative efficiency of 0.1, continuity in the accretion flow means that the product of the radial inflow velocity v_r and the relative thickness of the disk h/r is about 10^7 . Such a small value for this product means that we are dealing with a dense thin disk (h/r small) where the radial inflow velocity is much smaller than the tangential, Keplerian one, $v_r \ll v_\phi \sim c$. For an α -disk, $v_r \sim \alpha v_\phi (h/r)^2$, so $\alpha v_\phi (h/r)^3 \sim 3 \times 10^{-4}$. This is well satisfied if $\alpha \sim 0.3$ and $(h/r) \sim 0.1$ as expected for a standard thin disk. Of course, disk reflection only deals with the density near the surface of the disk; a higher mean disk density only strengthens the result. Thus, our reflection fits also strongly suggest that there is something approximating a standard thin disk at small radii.

We note that our results do not place strong constraints on the dominant hard X-ray emission mechanism(s). It is possible that thermal Comptonization, synchrotron emission, and synchrotron self-Comptonization all play important roles in defining the hard X-ray emission in the low-hard state. The apparent lack of a clear break or cut-off in the high energy spectrum may argue that thermal Comptonization is not the dominant emission mechanism, or may simply argue for a coronal electron temperature in excess of 100 keV.

3.7. Comparison with Cygnus X-1

In view of the remarkable results detailed above, we undertook a brief investigation of archival low-hard state Galactic black hole spectra. For this purpose, we selected the well-known source Cygnus X-1. While Cygnus X-1 caused photon pile-up in the *ASCA*/SIS detectors, robust spectra were obtained with the GIS gas detectors, which were well-calibrated over the 1.0–10.0 keV bandpass. *ASCA*/GIS spectra and response files available in the NASA public archive have been screened in accordance with the bright source considerations detailed in Brandt et al. (1996), and are ready for analysis. Observation 40027010 was obtained on 11 November 1993 starting at 01:37:04; the GIS-3 spectrum considered here has a net exposure time of 38 ksec.

Assuming a standard value for the column density along the line of sight to Cygnus X-1 ($N_H = 6.2 \times 10^{21} \text{ cm}^{-2}$; Miller et al. 2002b), a power-law fit to the spectrum above 3.0 keV yields a $\Gamma = 1.77$ photon power-law index typical of the low-hard state in Cygnus X-1. Extending this power-law down to 1.0 keV reveals a strong cool accretion disk component like that found

in GX 339–4 (see Figure 9). Moreover, a broad, relativistic Fe K α emission line is revealed, which is again suggestive of a disk which extends to $6 GM/c^2$ or less (see Figure 10).

Before including a disk component, the best fit statistic that can be achieved with this power-law index is $\chi^2/\nu > 15,000/764$. Allowing the column density to float within 30% of the standard value, which is a common deviation between instruments, an improved fit was again found. Next including “diskbb” and “laor” line components each separately improved the fit at more than the 8σ level confidence. This simple model yielded the following parameters: $kT = 0.22(1)$ keV for $R_{in} = 5.8(6) R_g$ (assuming $d = 2.5$ kpc, $i = 30^\circ$, and $M = 10 M_\odot$, Miller et al. 2002b, Herrero et al. 1995), $E_{line} = 6.90(7)$ keV for $R_{line} = 6(2) R_g$, $W_{line} = 250(30)$ eV, $\Gamma = 1.85(5)$, and $\chi^2/\nu = 1317/759$. Again, radii inferred from disk continuum fits must be regarded cautiously, though in this case the radius is still broadly consistent with the ISCO after inner torque and hardening corrections are made (see Zimmerman et al. 2004; Merloni, Fabian, & Ross 2000). The fit is not formally acceptable due to instrumental response errors around 2 keV; however, the statistical need for disk and disk line components does not arise due to response issues.

To explore the low/hard state at a lower fraction of the Eddington limit, $L_X/L_{Edd} \simeq 0.001$, we began a new investigation of the *Chandra*/LETGS spectrum of XTE J1118+480 in the low–hard state (see McClintock et al. 2001, Miller et al. 2002c). There is potential evidence for a cool X-ray disk remaining at the ISCO in this spectrum also. However, to make a robust determination, remaining uncertainties in the instrumental response and spectrum itself must be investigated in full, and we will report on this analysis in a later paper.

4. DISCUSSION

4.1. On the Accretion Flow Geometry in the Low–Hard State

We have conducted an analysis of *XMM-Newton* and *RXTE* spectra of GX 339–4 in a low–hard state. Our results suggest that a standard cool accretion disk may extend to the innermost stable circular orbit in the low–hard state. In a brief analysis of archival *ASCA* spectrum, we find that similar results are readily obtained for Cygnus X-1. Moreover, a spectrum recently obtained from the black hole candidate SWIFT J1753.5–0127 (Miller, Homan, & Miniutti 2006) during the decline of its outburst appears to support this disk geometry. Although we observed GX 339–4 in a rising phase, SWIFT J1753.5–0127 was observed during outburst decline, and Cygnus X-1 is a persistent source, suggesting that disks may commonly remain at or close to the ISCO in bright phases of the low–hard state.

These results have a number of consequences. Transitions between low–hard and high–soft states in black hole binaries may not necessarily signal a change in inner disk radius. Moreover, in apparent contrast to the absence of jets in disk-dominated high–soft states (see, e.g., Fender, Belloni, & Gallo 2004), it may be possible to maintain a compact, steady jet while the disk remains at the innermost stable circular orbit. Homan et al. (2001) noted that state transitions may be partly related to changes in the corona; our results strengthens this suggestion.

The idea that a transition into the low–hard state marks the onset of an ADAF with a truncated inner disk (e.g., Esin, McClintock, & Narayan 1997) has become a near-paradigm in studies of accreting black holes. Our results suggest that an optically-thick accretion disk with properties closely related to

disks observed at higher inferred accretion rates can operate in the low–hard state. However, simple theoretical considerations suggest that it is very unlikely that a standard thin disk is part of the inner accretion flow in quiescence. Observational evidence also appears to rule-out the possibility of a standard accretion disk at the ISCO in quiescence (see, e.g., McClintock, Horne, & Remillard 1995). By extension, then, our findings suggest that the accretion flow geometry in quiescence may not be a simple extrapolation of the geometry of the flow in the low–hard state.

Fits to the spectra with reflection models reveal a covering fraction significantly less than unity (see Table 2), consistent with prior disk reflection fits in the low–hard state (e.g. Gierlinski et al. 1997). While a recessed disk would serve to give less disk reflection, this possibility is inconsistent with our results. A hard component which is mildly beamed away from the disk provides a plausible way to reconcile these findings.

Beloborodov (1999) described a model wherein the corona is fed by magnetic flares from the disk, and the height of such flares determines the nature of the corona. In the low–hard state, the flares reach mildly relativistic velocities ($v/c \simeq 0.3$), sufficient to mildly beam the hard X-ray emission away from the disk. A broadly similar scenario has been described by Merloni & Fabian (2002); in that work, the ability of a magnetically-dominated corona to launch jets is considered. These models may give insight into how disks might be connected to jets through a corona, and/or give a sense of how a corona might act as the base of a jet. Separately, the possible role of a jet in producing hard X-ray emission in the low–hard state has been discussed in detail. Markoff, Falcke, & Fender (2001) suggested that all of the hard X-ray emission in XTE J1118+480 may be due to the steady, compact jet implied by radio observations. Subsequent studies have focused more on the role of synchrotron self-Comptonization; in this sense, they partially bridge the gap between synchrotron-dominated jet models and traditional thermal Comptonization models of the corona. Markoff & Nowak (2004) have showed that the level of disk reflection predicted by jet-dominated emission models is consistent with observations.

While our deep observation of GX 339–4 may provide the most convincing evidence that a standard thin disk is important in the low–hard state, it is not the first such evidence. Prior reports of cool disks in the low–hard state have sometimes been overlooked and/or regarded skeptically. A cool soft excess in the low–hard state spectrum of Cygnus X-1 was previously reported by Ebisawa et al. (1996), in the same *ASCA* spectrum we considered above. The presence of a cool thermal component in the low–hard state of Cygnus X-1 can be traced back much farther: Barr & van der Woerd (1990) and Balucinska & Hasinger (1991) both reported that a soft excess was required to describe the low–hard state spectrum of Cygnus X-1. The interpretation of this component as a disk was complicated by the possibility that the black hole may partially accrete from the wind of its massive companion. However, such a wind is clearly not present in GX 339–4, and the evidence for a disk in the low–hard state of GX 339–4 supports the disk interpretation of the soft component in Cygnus X-1.

If a disk interpretation of this component was doubted because the black hole may partially accrete via the wind from its massive companion, the clear evidence for a disk in the low-mass binary GX 339–4 should make its interpretation clear.

It is likely that current views of the low–hard state have been heavily influenced by recent observations with *RXTE*. While

the flexibility of *RXTE* has made it possible to study the bright phases of accreting sources with densely-spaced observations, our results demonstrate that its effective lower energy threshold of 3 keV makes it insensitive to cool thermal components. For instance, Zdziarski et al. (2004) address the accretion flow as a function of state in GX 339–4 using *RXTE* data; Figure 10 in that work indicates that the disk suddenly and sharply changes its inner radius across state transitions. Such marked changes in apparent inner disk radius are more likely driven by instrumental limitations, and/or by modeling assumptions, than physical properties.

If a mechanism such as conduction can radially truncate a disk by driving rapid evaporation (e.g., Meyer-Hofmeister & Meyer 1999), it is clear that it does not necessarily activate with the transition to the low–hard state. In the absence of such a mechanism, a standard thin disk which is truncated interior to 50–100 R_g is not necessarily a stable configuration. Assuming an accretion efficiency of 10% and taking only the mass accretion rate implied by the disk flux in our observations of GX 339–4, the radial inward drift caused by viscosity in a standard disk, should transfer material to the innermost stable circular orbit from 50–100 R_g in approximately 10^3 s. While much longer than the free-fall time and the orbital timescale at 50–100 R_g , this drift timescale is still quite short, and serves to demonstrate how easily a disk can begin to fill an evacuated inner volume.

In future work on the low–hard state, it will be important to try to reconcile apparent UV disk components like that found in XTE J1118+480 (e.g., McClintock et al. 2001) with cool X-ray disk components. If the two cannot be reconciled, it is possible that soft X-ray excesses which appear to be cool disks may arise via other means. It is also possible that apparent UV disk components are not pure disk components, and possible that such components are not well understood. In a survey of UV spectra from short-period black hole binaries, Hynes (2005) finds that the spectra are generally steeper than the canonical $\nu^{1/3}$ disk spectrum, and that the broad-band optical spectra are consistent with power-law forms. Studies of the IR, optical, and UV variability observed from XTE J1118+480 in its low–hard state indicate a synchrotron origin for the variability (Hynes et al. 2003), suggesting that UV emission in the low–hard state is not solely due to a disk.

4.2. Reconciling Timing and Spectral Phenomena

It is sometimes argued that the low-frequency QPOs (on the order of 1 Hz, and lower) occasionally observed in the low–hard state, serve to indicate that the disk is radially recessed. Such arguments are largely based on the assumption that the low QPO frequency reflects the Keplerian orbital frequency of the inner disk. This inference would certainly contradict spectroscopic evidence that the inner disk extends to the ISCO, at least in the bright phases of the low–hard state. Since the nature of low frequency QPOs is an open question, it is not possible to entirely refute the possibility that these QPOs signal a recessed disk. A few simple considerations, however, argue against interpreting low-frequency QPOs as evidence for a recessed disk.

First, the QPOs observed are *X-ray* QPOs, and energetic arguments demand that accreting material release most of its energy in the inner few Schwarzschild radii. A disk truncated at several tens or hundreds of Schwarzschild radii, but which still contributes substantial X-ray emission, is problematic from the standpoint of producing strong X-ray oscillations in the *RXTE* bandpass. Embedding the disk in a Comptonizing corona might

solve this problem, and may even explain the fact that the strength of QPOs is often observed to increase with energy. However, in ADAF plus truncated disk models, most Comptonization occurs interior to the truncated disk, and embedding a disk in that volume is inconsistent with the basic premise of the model.

Second, although high frequency QPOs are apparently absent in the low–hard state, it is not necessarily appropriate to associate the Keplerian frequency at the inner disk with low-frequency QPOs. Low-frequency QPOs similar to those found in low–hard states are often observed *simultaneously* with high-frequency QPOs in the “very high” and “intermediate” states (also known as “steep power-law” states, or, more generically, bright hard states; see McClintock & Remillard 2005). In such cases, low-frequency QPOs are *not* used to infer the inner disk radius; it is inconsistent to interpret low-frequency QPOs in this way in the low–hard state. We note that it is possible that high frequency QPOs are actually present in the low/hard state, but have simply not been detected due to a lack of sensitivity. We know of no work which has demonstrated that high frequency QPOs are absent in the low/hard state, at an rms upper limit similar to the rms at which high-frequency QPOs are detected in other states. Far tighter limits will be required to also rule-out the possibility that the high frequency QPO formation mechanism depends more strongly on the mass accretion rate than the inner disk radius.

These considerations do not argue against the possibility that QPO frequency trends (see, e.g., Rossi et al. 2004, Belloni et al. 2005) signal a real geometrical change in black hole systems. It is possible that changes in the size of the corona, the distance between the inner disk and jet, the scale height of flares above the disk, or the timescale for superorbital variations in the disk itself may be reflected in such frequency trends. A large number of simultaneous multi-wavelength observations of black holes in the near future may help to reveal the nature of low frequency QPOs.

4.3. On Disk–Jet Connections in Black Holes

Fender, Belloni, & Gallo (2004) have recently proposed a broad model for jet production in black hole binary systems. This model succeeds in accounting for many of the observed radio and X-ray properties in these systems. Among the most important things any such model needs to address, is the ubiquitous production of jets in low–hard states, and the absence of jets in high–soft states, when the disk is strongest. Indeed, the absence of jets in the most disk–dominated states demonstrates that disk–jet coupling may be complex.

Within the current framework of the Fender, Belloni, & Gallo (2004) model, the absence of jet production in the high–soft state is associated with a smaller inner disk radius in this state. Our results indicate that the inner disk radius may not change across state transitions, and suggest that another parameter is likely responsible for quenching jets in the high–soft state. For instance, if the corona is central to driving jets, the ratio of energy dissipated in the corona to that dissipated in the disk may be critical. A corona which is efficiently cooled below a certain electron temperature by the disk may be less able to drive jets than a very hot corona. Detailed spectroscopy across a black hole outburst could test whether or not the empirical “jet line” found in hardness–intensity diagrams can be explained in terms of this ratio. This parameter, and others, may naturally fit within the larger framework of the Fender, Belloni, & Gallo (2004) model.

It is also possible that there may be *no* simple disk–jet connection in accreting black holes. It has already been noted that if the jet has any role to play in X-ray emission, correlations between radio and X-ray luminosity may not be disk–jet connections, but jet–jet connections (Markoff et al. 2003). If the jet does not play a significant role in X-ray emission, such relations may portray corona–jet connections (though if the corona is indeed the base of a jet, whether such relations represent jet–jet connections or corona–jet connections is largely a question of semantics). Our results also suggest that there is no clear relation between hard X-ray emission and inner disk radius, regardless of the hard X-ray emission mechanism, so any corona–jet connections could be quite independent of the inner radius of the disk.

4.4. Implications for Low-luminosity AGN and LINERs

It is sometimes suggested that stellar-mass black holes in the low–hard state, and low-luminosity AGN (LLAGN) and LINERs may have a common inner accretion flow geometry (e.g., Markowitz & Uttley 2005). Although many LLAGN are likely observed at lower Eddington fractions (10^{-5} – 10^{-4}) than the range covered by the three stellar-mass black hole observations considered in this work, if LLAGN are truly supermassive black holes in the low–hard state, our results suggest that the accretion disks in these sources may also remain at the ISCO. This suggestion adds to recent evidence that disks are not dramatically recessed in LLAGN and LINERs. Maser emission from the accretion disk in NGC 4258 demands that any inner advective region can be no larger than $100 R_{Schw}$. (Herrnstein et al. 1998). Moreover, a recent UV variability study has detected emission which can be associated with a disk in a number of LINERs (Maoz et al. 2005). Extremely deep X-ray observations of nearby LLAGN such as M81* and NGC 4258 may be required to determine whether the disks in these sources are recessed, or if they remain at the ISCO.

5. CONCLUSIONS

A long *XMM-Newton* observation of GX 339–4 has demonstrated that a standard thin accretion disk can remain at the innermost stable circular orbit around a black hole in the low–hard state. This finding has a few important consequences. Advection-dominated accretion flows with truncated thin disks may be important at very low fractions of the Eddington limit, but do not appear to describe the low–hard state at $L_X/L_{Edd} \geq 0.01$. Similarly, our results suggest the production of steady compact jets in the low–hard state, and the quenching of jets in the high–soft state, are phenomena unrelated to the inner radius of the accretion disk. Finally, our spectral results provide additional support for envisioning the hard X-ray emitting “corona” as being related to the base of a jet.

We thank Omer Blaes, Michael Garcia, Rob Fender, Sera Markoff, Jeff McClintock, Ramesh Narayan, Mike Nowak, Chris Reynolds, and Henk Spruit for stimulating discussions. We thank Patrick Woudt, Retha Pretorius, Tetsuya Nagata, and Ikuru Iwata for their contributions to the multi-wavelength campaign. We thank the anonymous referee for constructive comments which improved the paper. JMM acknowledges research funding related to this program from NASA. DS acknowledges support through the Smithsonian Astrophysical Observatory Clay Fellowship. This work is based on observations obtained with *XMM-Newton*, an ESA mission with instruments and contributions directly funded by ESA member states and the US (NASA). The Australia Telescope Compact Array is part of the Australia Telescope which is funded by the Commonwealth of Australia for operation as a National Facility managed by CSIRO. This work has made use of the tools and services available through HEASARC online service, which is operated by GSFC for NASA.

REFERENCES

- Arnaud, K. A., and Dorman, B., 2000, XSPEC is available via the HEASARC on-line service, provided by NASA/GSFC
- Ballantyne, D., Iwasawa, K., & Fabian, A. C., 2001, *MNRAS*, 261 74
- Balucinka, M., & Hasinger, G., 1991, *A&A*, 241, 439
- Baganoff, F., et al., 2003, *ApJ*, 591, 891
- Barr, P., White, N. E., & Page, C. G., 1985, 216, 65
- Barr, P., & van der Woerd, H., 1990, *ApJ*, 352, L41
- Belloni, T., & Hasinger, G., 1990, *A&A*, 227, L33
- Belloni, T., Mendez, M., King, A. AR., van der Klis, M., & van Paradijs, J., 1997, *ApJ*, 479, L145
- Belloni, T., et al., 2005, *A&A*, 440, 207
- Beloborodov, A. M., 1999, *ApJ*, 510, L123
- Brandt, W. N., Fabian, A. C., Dotani, T., Nagase, F., Inoue, H., Kotani, T., & Segawa, Y., 1996, *MNRAS*, 293, 1071
- Done, C., & Gierlinksi, M., 2006, *MNRAS*, in press
- Esin, A. A., McClintock, J. E., & Narayan, R., 1997, *ApJ*, 489, 865
- Fabian, A. C., et al., 1995, *MNRAS*, 277, L11
- Fender, R. P., 2005, in “Compact Stellar X-ray Sources”, eds. W. H. G. Lewin and M. van der Klis, Cambridge University Press, Cambridge
- Frank, J., King, A., & Raine, D., 2002, in “Accretion Power in Astrophysics”, Cambridge University Press, Cambridge
- Gallo, E., Corbel, S., Fender, R. P., Maccarone, T. J., & Tzioumis, A. K., 2004, *MNRAS*, 347, L25
- Gierlinksi, M., et al., 1997, *MNRAS*, 288, 958
- Greisen, E., 2005, ed.: AIPS Cookbook; <http://www.aoc.nrao.edu/aips/cook.html>
- Herrero, A., Kudritzki, R. P., Gabler, R., Vilchez, J. M., & Gabler, A., 1995, *A&A*, 297, 556
- Herrnstein, J. R., Greenhill, L. J., Moran, J. M., Diamond, P. J., Inoue, M., Nakai, N., & Miyoshi, M., 1998, *ApJ*, 497, L69
- Meyer-Hofmeister, E., & Meyer, F., 1999, *A&A*, 348, 154
- Homan, J., et al., 2001, *ApJS*, 132, 377
- Homan, J., & Belloni, T., 2004, to appear in the Proc. of “From X-ray Binaries to Quasars: Black Hole Accretion on All Mass Scales”, ed. T. J. Maccarone, R. P. Fender, L. C. Ho (Dordrecht: Kluwer), astro-ph/0501186
- Homan, J., Buxton, M., Markoff, S., Bailyn, C. D., Nespoli, E., & Belloni, T., 2005, *ApJ*, 624, 295
- Hynes, R. I., Steeghs, D., Casares, J., Charles, P. A., & O’Brien, K., 2003, *ApJ*, 583, L95
- Hynes, R. I., Steeghs, D., Casares, J., Charles, P. A., & O’Brien, K., 2004, *ApJ*, 609, 317
- Hynes, R. I., 2005, *ApJ*, 623, 1026
- Hynes, R. I., et al., 2006, *ApJ*, in press, astro-ph/0607314
- Klein-Wolt, M., & van der Klis, M., 2004, *Nucl. Phys. B Proceedings Supplements*, 132, 381
- Maccarone, T., 2002, *MNRAS*, 336, 1371
- Magdziarz, P., & Zdziarski, A. A., 1995, *MNRAS*, 273, 837
- Maoz, D., Nagar, N. M., Falcke, H., & Wilson, A. S., 2005, *ApJ*, 625, 699
- Markoff, S., Falcke, H., & Fender, R. P., 2001, *A&A*, 372, L25
- Markoff, S., & Nowak, M. A., 2004, *ApJ*, 609, 972
- Markoff, S., Nowak, M. A., & Wilms, J., 2005, *ApJ*, 635, 1203
- Markowitz, A., & Uttley, P., 2005, *ApJ*, 625, L39
- McClintock, J. E., Horne, K., & Remillard, R. A., 1995, *ApJ*, 442, 358
- McClintock, J. E., & Remillard, R. A., 2005, to appear in “Compact Stellar X-ray Sources” eds. W. H. G. Lewin and M. van der Klis, Cambridge: Cambridge University press, astro-ph/0306213
- McClintock, J. E., et al., 2001, *ApJ*, 555, 477
- Merloni, A. A., & Fabian, A. C., 2002, *MNRAS*, 332, 165
- Merloni, A. A., Fabian, A. C., & Ross, R. R., 2000, *MNRAS*, 313, 193
- Miller, J. M., Ballantyne, D. R., Fabian, A. C., & Lewin, W. H. G., 2002, *MNRAS*, 335, 864
- Miller, J. M., et al., 2002a, *ApJ*, 570, L69
- Miller, J. M., et al., 2002b, *ApJ*, 578, 348
- Miller, J. M., et al., 2002c, *MNRAS*, 335, 865
- Miller, J. M., et al., 2004a, *ApJ*, 601, 450
- Miller, J. M., et al., 2004b, *ApJ*, 606, L131
- Miller, J. M., Homan, J., & Miniutti, G., 2006, *ApJ*, subm., astro-ph/0605190
- Miyamoto, S., Kimura, K., Kitamoto, S., Dotani, T., & Ebisawa, K., 1991, *MNRAS*, 383, 748

- Miyamoto, S., Kitamoto, S., Hayashida, K., & Egoshi, W., 1995, *ApJ*, 442, L13
Park, S. Q., et al., 2004, *ApJ*, 610, 378
Reynolds, C. S., & Wilms, J., 2000, *ApJ*, 533, 821
Rossi, S., Homan, J., Miller, J. M., & Belloni, T., 2005, *MNRAS*, 360, 763
Sault, R., & Killeen, N., 2004, *Miriad Users Guide*; <http://www.atnf.csiro.au/computing/software/miriad>
Shakura, N. I., & Sunyaev, R. A., 1973, *A&A*, 86, 121
Shimura, T., & Takahara, F., 1995, *ApJ*, 445, 780
Shrader, C., & Titarchuk, L., 1999, *ApJ*, 511, 289
Tanaka, Y., et al., 1995, *Nature*, 375, 659
Titarchuk, L., Kazanas, D., & Becker, P. A., 2003, *ApJ*, 598, 411
Vadawale, S., Rao, A. R., Naik, S., Yadav, J. S., Ishiwara-Chandra, C. H., Pramesh Rao, A., & Pooley, G. G., 2003, *ApJ*, 597, 1023
Vaughan, S., & Fabian, A. C., 2004, *MNRAS*, 348, 1415
Zdziarski, A. A., Gierlinski, M., Mikolajewska, J., Wardzinski, G., Smith, D. M., Harmon, A., & Kitamoto, S., 2004, *MNRAS*, 351, 791
Zimmerman, E. R., Narayan, R., McClintock, J. E., & Miller, J. M., 2005, *ApJ*, 618, 832

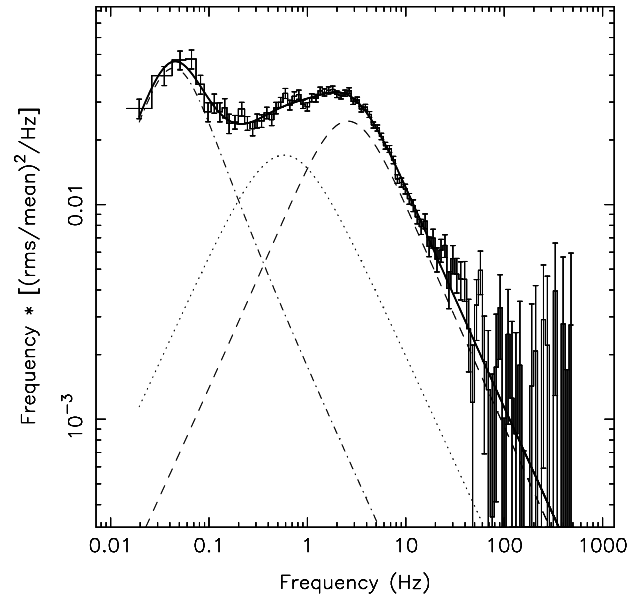


FIG. 1.— A power density spectrum of GX 339-4 obtained with *RXTE* during the long *XMM-Newton* observation is shown above. This power spectrum is typical of the low-hard state, in that it shows high fractional variability and band-limited noise. The power spectrum was fit with three Lorentzians ($\chi^2/\nu = 204/177$) shown with dashed and dotted lines.

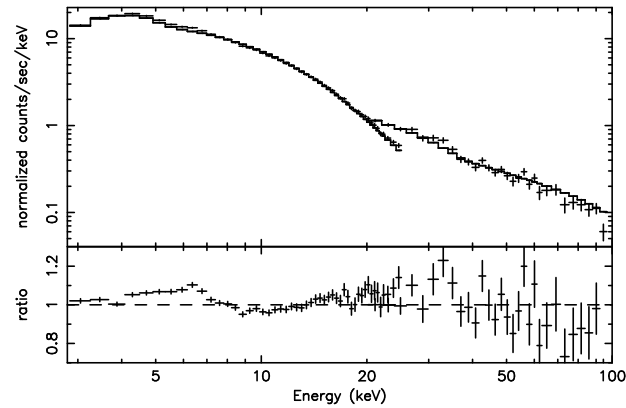


FIG. 2.— A simple absorbed power-law fit to *RXTE* spectra of GX 339-4 is shown above. The 4.0–7.0 keV region was ignored during the fit. The *RXTE* continuum is clearly well-described by this simple phenomenological function, with no clear evidence of a break or cut-off in the spectrum. Evidence for a broad Fe K line can be seen in the data/model ratio. The lack of obvious curvature near 30 keV indicates that any disk reflection is likely to be relatively weak.

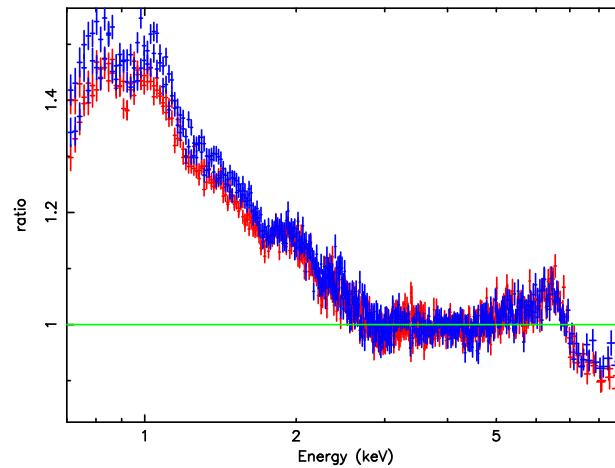


FIG. 3.— The ratio of the *XMM-Newton* spectra of GX 339-4 when fit with a power-law in the 3-10 keV band are shown above. Spectra from revolution 782 are shown in red; spectra from revolution 783 are shown in blue. The soft thermal excess can be fit with an accretion disk which extends to the ISCO, indicating that the disk is not radially recessed in the low-hard state. *RXTE*, with an effective lower energy bound of 3 keV, has failed to detect such disk components because the disk contributes minimal flux above 3 keV.

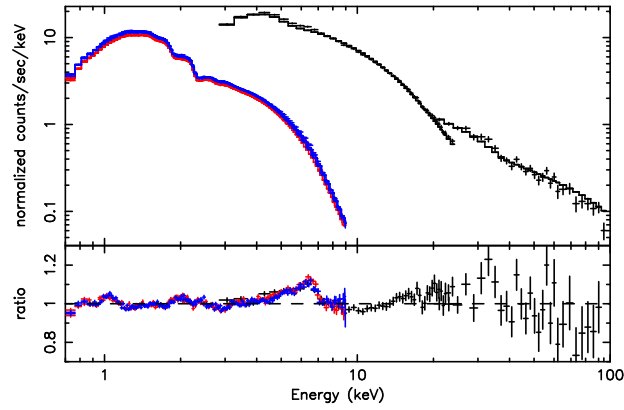


FIG. 4.— *XMM-Newton* and *RXTE* spectra of GX 339–4 are shown above, fit jointly with a simple absorbed disk plus power-law model. *XMM-Newton* spectra from revs. 782 and 783 are shown in blue and red, respectively, and the *RXTE* spectra are shown in black. The 4.0–7.0 keV band was ignored in fitting the spectra. The broad Fe K line is common between the instruments, and is clearly revealed in the *XMM-Newton* spectra.

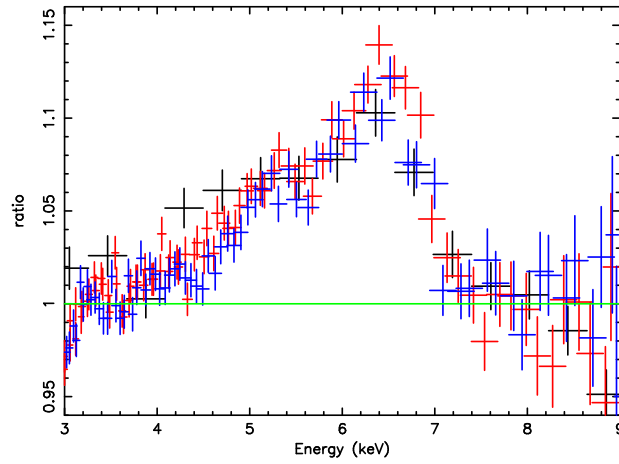


FIG. 5.— The relativistic Fe K line revealed in Figure 4 is shown in detail above. The plot shown above was made in a manner chosen to prevent biasing the line profile. The model was a simple disk plus power-law model, and the 4.0–7.0 keV region was ignored in fitting the data. *XMM-Newton* data from revs. 782 and 783 are shown in red and blue, respectively, and the *RXTE* spectrum is shown in black.

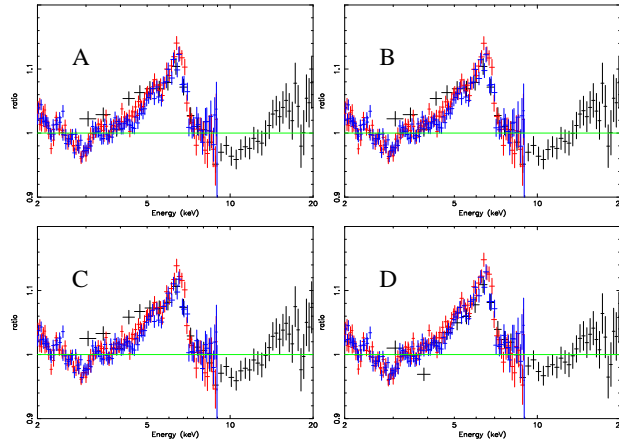


FIG. 6.— The relativistic line profile observed in the low-hard state of GX 339–4 is remarkably independent of the continuum assumed. *XMM-Newton* spectra from revs. 782 and 783 are shown in red and blue, respectively, and the *RXTE* spectra are shown in black. In panel A, the standard “diskbb” plus power-law continuum model was used to form the data/model ratio. In panel B, a different disk model, “diskpn”, was used. In panel C, the “compTT” Comptonization model was used instead of a power-law. In panel D, the “bulk motion Comptonization” model was used instead of both additive components. In all cases, the 4.0–7.0 keV band was ignored in fitting the spectra.

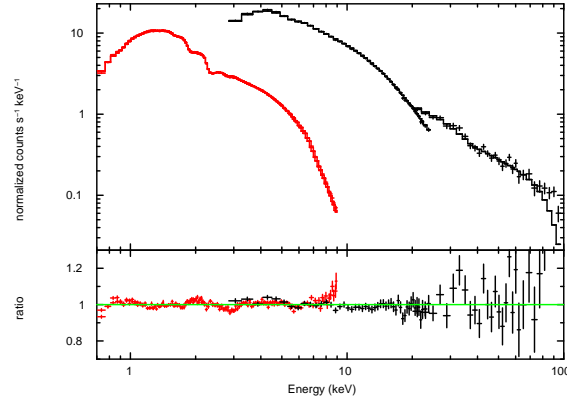


FIG. 7.— The plot above shows the result of joint spectral fits to the simultaneous *XMM-Newton* and *RXTE* spectra with the “constant density ionized disk” reflection model on the 0.7–100.0 keV band. The disk reflection spectrum was relativistically “blurred” with the line function expected from a disk around a Kerr black hole. The fit indicates a low reflection fraction, $f \simeq 0.3$ (where $f \propto \Omega/2\pi$), yet demands that the disk is within $5 GM/c^2$ of the black hole. This fit suggests that the hard X-ray component which illuminates the disk may not be isotropic, but may be mildly beamed away from the disk, as per the base of a jet.

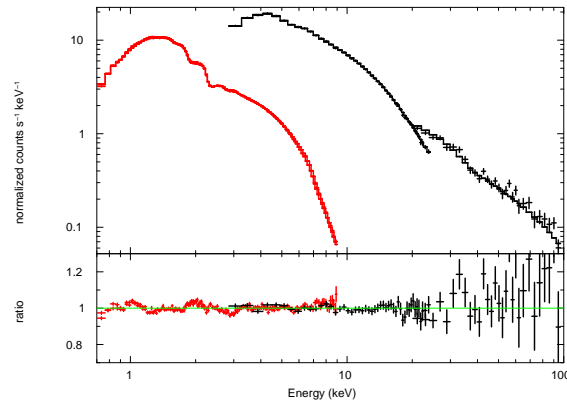


FIG. 8.— The plot above shows the result of joint spectral fits to the simultaneous *XMM-Newton* and *RXTE* spectra with the “pexriv” disk reflection model. The results of this model confirm those obtained with the “constant density ionized disk” model, in that a low reflection fraction and a disk close to the ISCO is required to describe the data. This result also suggests that the “corona” may be base of a mildly relativistic jet which weakly beams the hard X-ray emission.

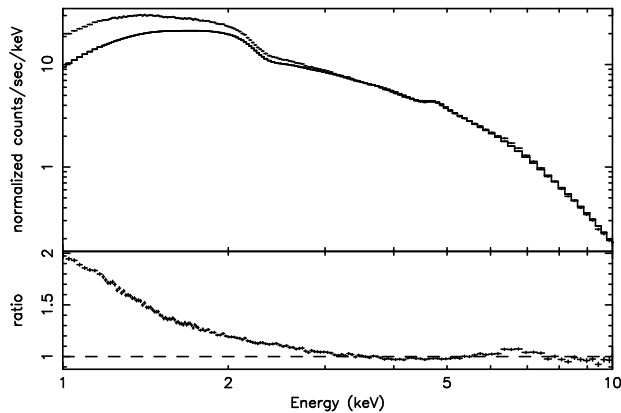


FIG. 9.— The plot above shows an *ASCA*/*GIS* spectrum of Cygnus X-1 in the low-hard state, fitted with a simple power-law in the 3.0–10.0 keV band. Similar to the *XMM-Newton* spectra of GX 339–4, a soft excess is revealed that is consistent with a cool accretion disk at the ISCO.

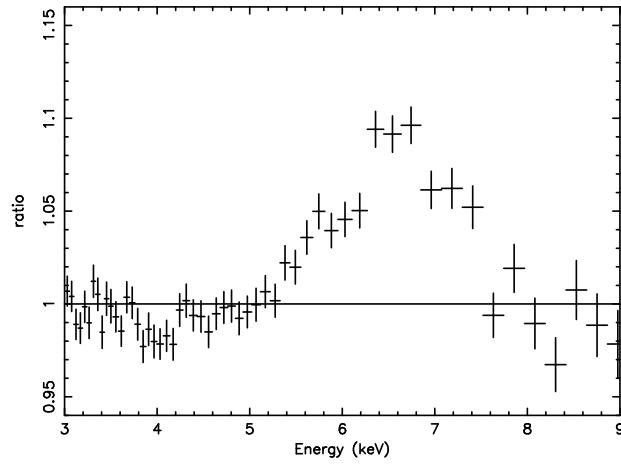


FIG. 10.— The plot above shows the ratio of an *ASCA*/GIS spectrum of Cygnus X-1 in the low-hard state, fitted with a simple absorbed disk blackbody plus power-law model. The 4.0-7.0 keV region was ignored in fitting the spectrum. Similar to the *XMM-Newton* observation of GX 339-4, a broad, relativistic Fe K line is revealed. Fits to the line suggest that it originates at radii consistent with the ISCO, again demanding the disk is not recessed in the low-hard state of Cygnus X-1.

TABLE 1

Joint Spectral Fits with Simple Models

	diskbb + power-law	diskpn + power-law	diskbb + compTT	bulk. mot. compt.
N_H (10^{21} cm $^{-2}$)	3.72(5)	3.73(4)	3.1(1)	3.0(1)
kT_{disk} (keV)	0.38(1)	0.36(2)	0.29(1)	–
R_{disk} (R_g)	2.4(2)	6.0	5(3)	–
N_{disk}	640(80)	0.011(2)	2700(400)	–
E_{line} (keV)	6.85(5)	6.90(5)	6.85(5)	6.92(5)
q_{line}	3.3(1)	3.3(1)	3.3(1)	3.3(1)
R_{line} (R_g)	2.8(2)	2.8(2)	3.1(2)	3.1(2)
i (deg)	18(5)	18_{-8}^{+6}	24(8)	19(9)
N_{line} (10^{-3})	7.4(5)	7.3(5)	7.6(5)	8.0(7)
W_{line} (eV)	350(20)	350(20)	360(20)	380(40)
Γ	1.46(1)	1.46(1)	–	–
kT_0	–	–	0.27(1)	0.26(1)
kT_e	–	–	21(2)	–
τ	–	–	2.8(1)	–
α	–	–	–	0.48(1)
$\log(A)$	–	–	–	0.80(2)
N_{hard}	0.320(5)	0.320(5)	0.042(3)	0.0150(2)
χ^2/ν	3899.2/2256	3905.9/2256	4071.0/2255	4103.1/2259

NOTE.—The table above details the results of fitting simple spectral models to all four *XMM-Newton*/EPIC-MOS and two *RXTE* PCA and HEXTE spectra jointly with simple continuum models. The “diskbb” model is the standard multicolor disk model, and the “diskpn” model is a variation which assumes a pseudo-Newtonian inner potential (see Zimmerman et al. 2005 for a discussion). The “Laor” disk line component was used in the above models. Inner disk radii inferred via the disk continuum models assume $i = 18^\circ$ and a distance of 8.5 kpc, and are subject to various systematic errors (see the text). Unlike the other three models, the “bulk motion Comptonization” model is a single continuum, and does not contain a separated disk component. Symmetric errors are given in parentheses; single-digit errors indicate the error in the last significant digit for the given parameter value.

TABLE 2

Joint Spectral Fits with Relativistically-blurred Disk Reflection Models

	const. dens. ion. disk	pexriv
N_H (10^{21} cm $^{-2}$)	4.4(4)	3.7(4)
kT_{disk} (keV)	0.30(4)	0.39(4)
R_{disk} (R_g)	–	–
N_{disk}	2100(200)	700(200)
E_{line} (keV)	–	6.8(1)
$q_{line/blur}$	3.0	3.0
$R_{line/blur}$ (R_g)	5.0(5)	4.0(5)
i (deg.)	20_{-10}^{+5}	20_{-15}^{+5}
N_{line} (10^{-3})	–	3.5(3)
Γ	1.50	1.41(3)
$f \propto \Omega/2\pi$	0.31(3)	0.22(6)
$\log(\xi)$	2.8(1)	3.0
N_{hard}	$1.9(3) \times 10^{-25}$	0.32(3)
χ^2/ν	2055.1/1165	2120.5/1160

NOTE.—The table above details the results of jointly fitting relativistically-blurred disk reflection models to the two *XMM-Newton*/EPIC-MOS spectra from revolution 782 and two *RXTE* PCA and HEXTE spectra. Symmetric errors are given in parentheses. Single-digit errors indicate the error in the last significant digit for the given parameter value. The constant density ionized reflection model includes line emission, and a separate line component was not included in the overall spectral model. The pexriv model does not include a line, and its blurring parameters were tied to those of a “Laor” line included in the overall spectral model. Where errors are not given, the parameter was fixed at the quoted value.